Precision Agriculture (2020) 21:51–76
https://doi.org/10.1007/s11119-019-09659-5

Assessment of maize yield and phenology by drone-mounted superspectral camera

Ittai Herrmann[1] · Eyal Bdolach[2,3] · Yogev Montekyo[3] · Shimon Rachmilevitch[4] · Philip A. Townsend[5] · Arnon Karnieli[2]

Published online: 4 April 2019

Abstract

The capability of unmanned aerial vehicle (UAV) spectral imagery to assess maize yield under full and deficit irrigation is demonstrated by a Tetracam MiniMCA12 11 bands camera. The MiniMCA12 was used to image an experimental field of 19 maize hybrids. Yield prediction models were explored for different maize development stages, with the best model found using maize plant development stage reproductive 2 (R2) for both maize grain yield and ear weight (respective R^2 values of 0.73 and 0.49, and root mean square error of validation (RMSEV) values of 2.07 and 3.41 metric tons per hectare using partial least squares regression (PLS-R) validation models). Models using vegetation indices for inputs rather than superspectral data showed similar R^2 but higher RMSEV values, and produced best results for the R4 development stage. In addition to being able to predict yield, spectral models were able to distinguish between different development stages and irrigation treatments. These abilities potentially allow for yield prediction of maize plants whose development stage and water status are unknown.

Keywords Maize · Yield assessment · Phenotyping · Partial least squares · UAV · VENμS

Electronic supplementary material The online version of this article (https://doi.org/10.1007/s11119-019-09659-5) contains supplementary material, which is available to authorized users.

✉ Ittai Herrmann
Ittai.Herrmann@mail.huji.ac.il

[1] The Robert H. Smith Institute of Plant Sciences and Genetics in Agriculture, Hebrew University of Jerusalem, 7610001 Rehovot, Israel

[2] The Remote Sensing Laboratory, Jacob Blaustein Institutes for Desert Research, Ben-Gurion University of the Negev, 8499000 Beersheba, Israel

[3] Evogene Ltd., 7612002 Rehovot, Israel

[4] French Associates Institute for Agriculture and Biotechnology of Drylands, The Jacob Blaustein Institutes for Desert Research, Ben-Gurion University of the Negev, 8499000 Beersheba, Israel

[5] Department of Forest & Wildlife Ecology, University of Wisconsin-Madison, Madison, WI 53706, USA

Abbreviations

ASD	Analytical spectral devices
CC	Canopy cover
CMOS	Complementary metal oxide semiconductor
CO_2	Carbon dioxide
GCPs	Ground control points
GNDVI	Green Normalized Difference Vegetation Index
GNSS	Global navigation satellite system
ILS	Incident light sensor
LAI	Leaf area index
NDREI	Normalized Difference Red-Edge Index
NDVI	Normalized Difference Vegetation Index
NGRDI	Normalized Green Red Difference Index
NIR	Near-infrared
OSAVI	Optimized soil adjusted vegetation index
PAR	Photosynthetically active radiation
PLS-DA	Partial least squares discriminant analysis
PLS-R	PLS regression
PW2	PixelWrench2
R	Reproductive
R^2	Coefficient of determination
RARSa	Ratio analysis of reflectance spectra chlorophyll a
RARSb	Ratio analysis of reflectance spectra chlorophyll b
RARSc	Ratio analysis of reflectance spectra carotenoid
REIP	Red-edge inflection point
RGB	Red, green and blue
RMSE	Root mean square error
RMSEC	RMSE for calibration
RMSECV	RMSE for cross validation
RMSEV	RMSEC for validation
rRMSE	Relative RMSE
RTK	Real time kinematic
RWC	Relative water content
SIPI	Structure insensitive pigment index
SR	Simple ratio
t/ha	Tons per hectare
TCARI	Transformed Chlorophyll Absorption Reflectance Index
TGI	Triangular Greenness Index
TVI	Triangular Vegetation Index
UAV	Unmanned aerial vehicles
V	Vegetative
VENμS	Vegetation and Environmental New micro Spacecraft
VIP	Variable importance in projection
VIs	Vegetation Indices
VT	Vegetative tasseling

Introduction

Maize (*Zea mays* L.) is grown in most countries around the world (Araus et al. 2012). It is one of the most important crops, serving as a source of food, fuel and animal feed (Yin et al. 2015). Based on FAO 2016 data, maize follows only sugar cane (raw cane—harvested with relatively high water content) and wheat, among all crops, in terms of global production and global area harvested, respectively (FAO, 2016). Maize grain yield has risen approximately 2% per year from the late 1930s into the twenty-first century, with this growth attributed to increased biotic and abiotic stress tolerance through improvements primarily in genetics ranging from 50 to 60% (Duvick 2005) to 75% (Tollenaar and Lee 2006; Araus et al. 2012) and agronomical practices are responsible to the remainder (Tollenaar and Lee 2006; Araus et al. 2012). It is important to mention that breeding and management interacts with each other, neither factor could have raised yields by itself (Duvick 2005).

Global climate variability can cause and enhance abiotic stresses (e.g., drought) that adversely impact crops and reduce yields. Climate variability influences maize yield in roughly 70% of maize harvesting regions (Ray et al. 2015), thus constituting an important food security issue. Long et al. (2006) noted that elevated atmospheric carbon dioxide (CO_2) levels are predicted to offset yield reduction due to increased temperature and declines in soil moisture. Nevertheless, in the absence of drought, maize yield is not expected to increase with rising CO_2 (Leakey et al. 2006). Therefore, developing climate resilient crop genotypes is imperative to ensure global food security (Mickelbart et al. 2015). Maize's spread from tropical into northern and southern temperate areas has prompted Gore et al. (2009) to suggest that the future of maize improvement will require including germplasm from all over the globe to take advantage of genetic information related to climate adaptations.

Improvements through breeding involve phenotyping and trait assessments, especially the assessment of yield potential in drought-affected field-grown plants (Andrade-Sanchez et al. 2014). Such breeding experiments typically employ a large number of varieties each planted in respective plots of only a few meters in size. Crop phenotyping is currently a bottleneck in plant research (Kirchgessner et al. 2016) and requires the development of new methods to obtain and assess traits from these many different experimental plots planted cover small areas. Grain yield is considered to be among the most useful traits that can be predicted from spectral data (Weber et al. 2012).

The interaction of light (from sunlight) with plant canopies is influenced by chemical and physical properties of the vegetation that influence absorption, transmittance and reflectance at different wavelengths (Townsend et al. 2016), and thus create the unique spectral signature of different species and phenotypes (Jetz et al. 2016). Where there is sufficient variability in the pool of chemical/structural traits related to growth traits drivers (e.g., pigment, water and nutrient content, leaf area index, leaf temperature, leaf inner structure and canopy structure), spectral data can then be expected to correlate with yield. The ability, then, to map traits spectrally from low-altitude aerial platforms such as unmanned aerial vehicles (UAVs; Colomina and Molina 2014) has become increasingly desirable in agricultural applications (Adao et al. 2017; Burkart et al. 2018). While numerous studies have tested mapping canopy vegetation traits through low altitude aerial phenotyping, few have explored maize grain yield assessment (Sankaran et al. 2015). Correlations of maize grain yield with vegetation indices (VIs) using red, green, blue and near-infrared (NIR) broad band data have been explored at multiple growth stages (Shanahan et al. 2001), including regression with the normalized difference vegetation index (NDVI) using data from a

handheld multispectral point sensor (with bands of 660 and 767 nm) collected during the vegetative part of the growing season (Thomason et al. 2007). VIs calculated from UAV-acquired visible range (red, green and blue; RGB) images have also been combined with UAV-acquired crop height information to assess grain yield during vegetative development stages (Geipel et al. 2014). VIs obtained from an airplane-mounted color NIR (green, red and NIR) camera during maize's flowering stage have been correlated with grain yield (Farrell et al. 2018), and likewise, UAV-mounted color NIR. NIR and RGB cameras have been used by Zaman-Allah et al. (2015) to correlate NDVI and their own crop senescence index, respectively, with maize grain yield during the early reproductive part of the growing season. Ground-based hyperspectral data from a fiber point spectrometer (495–1853 nm) has also been collected post-anthesis to build partial least squares regression (PLS-R) models for grain yield assessment, using measurements at both the canopy and leaf levels (Weber et al. 2012).

In addition to maize grain harvest, a relatively new method of harvesting fresh ears while leaving aside the rest of the plant has recently gained popularity among dairy farmers in the American Midwest (Lizotte and Savoie 2013). These fresh harvested whole ears are known as snaplage and can be useful as dairy cattle feed (Akins and Shaver 2014; Ferraretto et al. 2018). As such, ear weight is another maize yield parameter that interests breeders and farmers but, to the best of the authors' knowledge, has not previously been correlated to spectral data. This study presents a UAV-based spectral method to predict maize yield, in terms of grain as well as ear weight, via PLS-R models and vegetation indices using 11-band imagery in the range of 400–1000 nm. Predictability at several plant development stages was assessed as part of a breeding experiment with the ultimate objective of identifying genotypes with superior drought-tolerant early growth stages. The overarching aim of the current study was to predict yield at multiple maize development stages by using an airborne superspectral (10 to 20 bands) camera. Thus, it comprised three components: (1) predict maize yield (grain and ear) from airborne spectral data; (2) identify the most reliable development stage for maize yield prediction; and (3) spectrally differentiate between maize development stages. Spectral data is useful for current plant traits assessment and since the current traits can affect the yield at harvest, it was hypothesized that spectral data can be useful for maize (grain and ear) yield assessment and this ability would improve as the plants are developing. During the plant development there physical and chemical changes in the plant, therefore, an additional hypothesis was that phenology could be spectrally detected.

Methodology

Study area and experimental design

The experimental plot was setup in the summer of 2015 at Evogene Ltd. farm (31.8833°N, 34.8437°E, 80 m above mean see level) near the city of Rehovot, in the coastal plain of Judea, Israel. The climate is Mediterranean, with very dry summers. Twenty commercial maize hybrids were planted on May 5, 2015 in a randomized block design of four replicates for each of two irrigation treatments numbering 160 plots in all. One of the varieties did not sprout well, nor did a single plot for another variety, resulting in a total of 151 plots for the superspectral image analyses (Fig. 1). Each block contained four adjacent plot rows by five separated plot columns. Each individual plot ran a length of 8 m and included

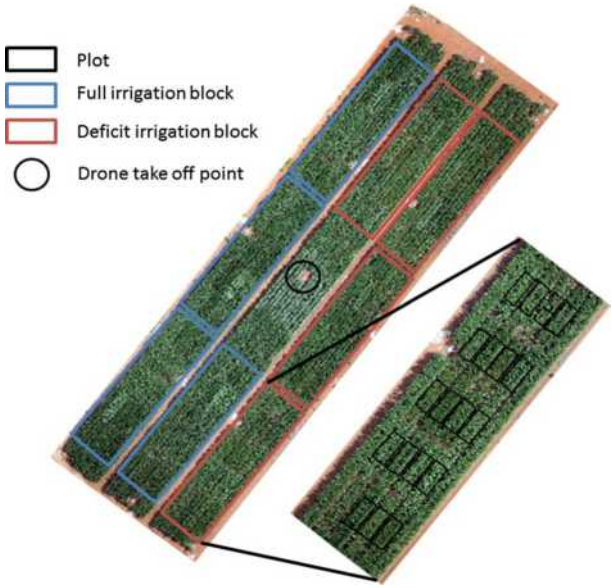

Fig. 1 The experimental field included four blocks fully irrigated and four blocks with deficit irrigation. In each block there were 19 plots. The image is of the V12 development stage. A color version of the figure is available on-line

two crop rows planted 0.8 m apart, at a density of roughly 8 plants per meter per row. To mitigate border effects, maize was planted next to each row that lacked adjacent maize plants, as well as around the entire experimental area. The experimental plots, border and fill plants were all planted by Miniair Profi630 (AHS Schoenmaekers, Valkenburg, Netherlands) on the same day. All seedlings were drip irrigated twice a week until they had eight fully open leaves, defined as development stage vegetative 8 (V8; Darby and Lauer 2006). After V8 the fully irrigated treatment was irrigated, twice a week as before while the deficit treatment's irrigation was reduced to once a week, cutting its total received water portion in half. Throughout the growing season, all destructive plant samples needed to determine traits were taken from the far ends of each plot, leaving the plot's middle undisturbed for the aerial spectral data collections.

Spectral data and plant trait measurements

Image acquisition utilized the MiniMCA12 (Tetracam Inc., Chatsworth, CA, USA) mounted on a self-made hexacopter. The MiniMCA12 camera consists of 12 cameras, each collecting one-band images that henceforth are referred to as bands. Each band records on a complementary metal oxide semiconductor (CMOS) detector with 1280×1024 pixels, with 11 for target imaging and one band as an upward-looking incident light sensor (ILS). Each of the 11 bands has a filter between the lens and the CMOS detector. The camera spectral bands are designed to simulate the 11 bands of the Israeli-French satellite Vegetation and Environmental New micro Spacecraft (VENμS) following by Herrmann et al. (2011): 420, 440, 490, 550, 640, 670, 700, 740, 780, 860 and 910 nm. The camera was mounted, under a vibration reducer, with 11 bands facing down. The ILS obtained radiation by two fiber optics that are connected to a foreoptics allowing it to be mounted apart from the main body of the camera, in the upper part of the UAV for full exposure to natural down-welling radiation. The ILS is used for reference measurements by the PixelWrench2

(PW2) software provided with the camera to retrieve reflectance from the digital number counts of the 11 upwelling bands.

Images were obtained on seven dates, one image per date, across the growing season (Table 1). All bands were pre-set to acquire images every 30 s using an integration time of 2.78 ms. The UAV launched from the same location on all dates (Fig. 1) and climbed vertically to 300 m above the ground. At this height the camera could capture the entire 130×40 m field, and analysis for each date was performed on a single selected full-view image as was also done by Farrell et al. (2018). The images were captured between 10:40 am and 01:00 pm.

Evogene Ltd. employees acquired and processed phenotypic data for the 19 maize hybrids across the full growing season. Information was obtained by destructive as well as non-destructive sampling as close as possible to the aerial imaging date (±2 days). Non-destructive sampling was done in the entire plot while destructive samples were collected from the first and last meter of the plot along the rows, allowing 6 m of undisturbed plot length to be analyzed from the air in conjunction with ground spectral and plant function data. The current study focused on spectral prediction of grain yield and ear dry weight from the airborne imagery. However, canopy cover (CC), relative water content (RWC) and leaf area index (LAI) were also measured throughout the growing season (Table 1) to assess their relationships with the grain yield and ear dry weight information. The grain and ear dry weight were obtained per 2 m in each row in the undisturbed part of the plot. Grain yield and ear weight, both in metric tons per hectare (t/ha) were obtained at the end of the growing season by destructive sampling in each of the 151 plots. Harvest was manual, with date of harvest ranging from August 11 to September 3, depending on the visually assessed developmental stage of each genotype. The ears were first dried at 65 °C for at least 48 h and weighed, and second threshed and again weighed. RWC was measured using leaf pieces from three plants per plot collected between 10:00 am and 2:00 pm one day prior to irrigation of both treatments. Fresh weight was measured immediately after sampling, then samples were hydrated in distilled water in the dark for one night to obtain their full turgid weight. These samples were likewise dried in an oven 65 °C for at least 48 h to determine the dry weight. The RWC is reported as the ratio between the difference of fresh weight and dry weight and the difference between turgid weight and dry weight (Barrs and Weatherley 1962). LAI was measured with the AccuPAR LP-80 ceptometer (Decagon Devices Inc., Pullman, WA, USA), calculated using the equations in the user manual (Decagon Devices 2016) based on the interception of photosynthetically active radiation (PAR) above and below the canopy (Norman and Jarvis, 1975). Measurements were acquired perpendicular to the rows in three areas of the undisturbed part of each plot and no more than two hours before or after mid-day (Herrmann et al. 2011). CC was calculated based on the same measurements as LAI by subtracting the below and above canopy PAR measurements ratio from bare soil represented as 1 (Decagon Devices 2016).

In vivo spectral data were obtained from leaves of five (32W86, Simon, CR5301 Cantabris, 47 and SC602) of the 19 hybrids (Fig. 2). In the undisturbed part of the relevant plots four plants (two from each row) were marked. An Analytical Spectral Devices (ASD) FieldSpec Pro FR spectrometer (ASD Inc., Boulder, CO, USA) was used to spectrally measure the marked plants at five development stages (Table 1). During the vegetative development stages (V6 and V10), the upper fully open leaf was measured. The leaf connected to the same node as the ear was measured at the vegetative tassel (VT; male maize flowers at the top of the canopy) development stage and reproductive (R) development stages R2 and R4 (Darby and Lauer 2006). The measurements were obtained on the upper side of the leaf, at the estimated center, between stem and tip of the leaf, and not on the central vein. ASD

Table 1 Data collection dates relate to development stage as well as irrigation treatment implementation and data type acquired

Development stage[a]	Date	Leaf level hyperspectral data	Aerial RGB images	Aerial superspectral MiniMCA12 images	CC	LAI	RWC	Days after previous irrigation	
								Full irrigation	Deficit irrigation
V4	May 25	−	+	+	+	+	−	1	1
V6	June 1	+	−	−	−	−	−	1	1
V6	June 2	−	+	+	+	+	−	2	2
V10	June 15	+	−	−	−	−	−	1	5
V10	June 16	−	+	+	+	+	+	2	6
V12	June 23	−	+	+	+	+	−	2	6
VT	July 6	+	−	−	+	+	−	1	5
VT	July 7	−	+	+	July 6	July 6	+	2	6
R2	July 17	−	+	+	−	−	−	2	2
R2	July 21	+	−	−	−	−	−	2	6
R4	July 27	+	+	+	July 29	July 29	+	1	5

The data obtained were spectral, canopy cover (CC), leaf area index (LAI) and relative water content (RWC), The symbols + and − respectively indicate data collection or no data collection for a given date

[a]Maize development stages are divided into vegetative (V) and reproductive (R) categories, separated by the vegetative tasseling (VT) stage

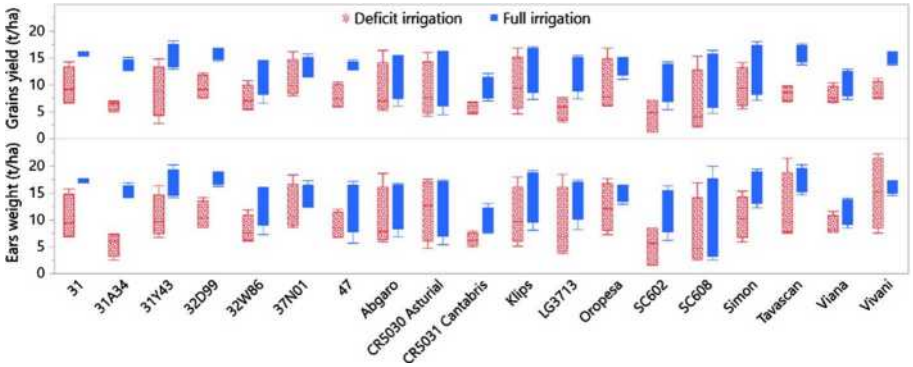

Fig. 2 Averaged yield values per variety and irrigation treatment, with standard error bars

spectral measurements at 350–2500 nm were acquired using an optic fiber connected to a contact probe (ASD Inc., Boulder, CO, USA) with tungsten halogen internal light source, using an average of 30 spectra for each sample measurement. A pure black plate with < 3% reflectance was placed behind the leaf during each measurement to reduce re-transmittance effects in the leaf measurements. Relative reflectance was calibrated and maintained by measuring a barium sulfate ($BaSO_4$) white reference panel at 15-min intervals, and all data were interpolated to 1 nm wavelength intervals.

Preprocessing superspectral images

The pixel size of MiniMCA12 images ranged from 179 mm to 191 mm depending on small variations in UAV flight altitude and the geo-correction process. The MiniMCA12 has 11 cameras for the 11 bands, thus requiring band alignment above what is offered in PW2 software (Rey-Carames et al. 2015; Laliberte et al. 2011) that is supplied with the MiniMCA12 as an image handling application tool for pre-processing and preliminary analyses. Thirteen ground control points (GCPs) marked by iron stakes were placed on the borders and inside the experimental field for the entire growing season, and geolocated using a Topcon GRS1 (Topcon Positioning Systems Inc., Livermore, CA, USA) real time kinematic (RTK) global navigation satellite system (GNSS). Plates with crosses were placed on the ground with each of the iron stakes in their center for each of the imaging dates. Each MiniMCA12 band was separately geo-corrected by the GCPs in ERDAS Imagine 2015 (Hexagon Geospatial, Norcross, GA, USA) with an accuracy of less than 48 mm (0.25 pixels) root mean square error (RMSE). A Sony A5100 (Sony Corporation, Tokyo, Japan) camera was flown 80 m above the ground to obtain RGB images on the same dates as the MiniMCA12 data collections (Table 1). These RGB images were processed to orthophoto mosaics in a Pix4D mapper software (Pix4D SA, Lausanne, Switzerland) environment. A shapefile, with one polygon for each plot was delineated from an early growing stages RGB orthophoto that was also used to georectify the MiniMCA12 images. ArcGIS 10.3 (Environmental System Research Institute, Redlands, CA, USA) was used to extract spectral data from the MiniMCA12 images, by the plot polygons, buffering 0.25 m from the plot edge and avoiding the disturbed 1 m ends. For analysis, spectral data were averaged for all pixels in each plot (average number of pixels per plot = 182.1).

Data analyses

Partial least squares regression (PLS-R) was used to predict yield from the superspectral data. PLS-R is widely used as a predictive tool for spectral reflective data (Hansen and Schjoerring 2003; Nguyen and Lee 2006) because it efficiently handles the multi-collinearity present among the predictors, bands and wavelengths, regardless of whether the number of bands or wavelengths is larger or smaller than the number of observations (Atzberger et al. 2010; Wold et al. 2001). PLS-R results in a vector of coefficients, one for each wavelength, that represent a predictive equation for the dependent variable of interest. Absolute magnitude and sign of the coefficient correspond to the relative importance and direction of relationship for a given wavelength. These are plotted to illustrate the relative importance of different bands or spectral regions. PLS-R was conducted in Matlab 7.6 (MathWorks, Natick, MA, USA) using the PLS-toolbox (Eigenvector, Wenatchee, WA, USA). All PLS-R models were calibrated and cross validated by a random set of approximately 70% of the samples and validated using the remaining ~ 30%. The quality of the models is assessed from coefficient of determination (R^2) values between the measured and predicted parameter for the calibration, cross validation and validation. Also presented is RMSE for calibration (RMSEC), cross validation (RMSECV) and validation (RMSEV), calculated following Wise et al. (2006). The relative RMSE (rRMSE; Ferrio et al. 2005) was calculated as the ratio between RMSE and the standard error of the observed mean value of the variable. The ultimate objective is to identify models that maximize R^2 and minimize RMSE (Barrett 1974).

Vegetation indices were calculated from the superspectral data (Table 2) to test common band combinations used for mapping. Pearson correlations were used to test relationships among variables, and regressions (again with a 70/30 calibration/validation split) were employed to test the quality of prediction by the indices (analyses conducted in Matlab 7.6), again using R^2 and RMSE to evaluate.

PLS discriminant analysis (PLS-DA) models were applied to classify spectral data to development stages of maize and irrigation treatments. PLS-DA relates the PLS (continuous) to the DA (categorical) by arbitrarily assigning each sample a numeric value indicating its class (Xie et al. 2007), which is converted to a set of binary class variables totaling the number of classes in the data (Musumarra et al. 2004). PLS-DA analyses were applied in a Matlab 7.6 environment using the PLS-toolbox. All PLS-DA utilized a 70/30 calibration/validation split, were evaluated using confusion matrices, and had their quality assessed by Cohen's Kappa (Cohen 1960), which downweights accuracy by proportion of agreement due to chance. The variable importance in projection (VIP) after Wold et al. (1993) was used to illustrate the relative importance of spectral bands or regions to the PLS-DA model.

Results and discussion

Yield assessment by PLS-R models

Grain yield, from all plots, ranged from 1.28 to 18.30 t/ha and the ear weight ranged from 1.60 to 22.25 t/ha (Fig. 2). As expected, yields declined under the deficit irrigation treatments, in agreement with Najafinezhad et al. (2015).

Table 2 Names, equations and references for common vegetation indices

Index	Name	Equation	Reference
SR	Simple ratio	$\frac{\rho_{780}}{\rho_{670}}$ (1)	Jordan (1969)
NDVI	Normalized Difference Vegetation Index	$\frac{\rho_{780}-\rho_{670}}{\rho_{780}+\rho_{670}}$ (2)	Rouse et al. (1973)
NGRDI	Normalized Green Red Difference Index	$\frac{\rho_{550}-\rho_{670}}{\rho_{550}+\rho_{670}}$ (3)	Tucker (1979)
REIP	Red-edge inflection point	$700+40\left\{\frac{[(\rho_{670}+\rho_{780})/2]-\rho_{700}}{\rho_{740}-\rho_{700}}\right\}$ (4)	Guyot and Baret, (1988)
RARSa	Ratio analysis of reflectance spectra chlorophyll a	$\frac{\rho_{670}}{\rho_{700}}$ (5)	Chappelle et al. (1992)
RARSb	Ratio analysis of reflectance spectra chlorophyll b	$\left(\frac{\rho_{670}}{\rho_{640}}\right)\rho_{700}$ (6)	Chappelle et al. (1992)
RARSc	Ratio analysis of reflectance spectra carotenoid	$\frac{\rho_{780}}{\rho_{490}}$ (7)	Chappelle et al. (1992)
NDREI	Normalized difference red-edge index	$\frac{\rho_{780}-\rho_{740}}{\rho_{780}+\rho_{740}}$ (8)	Gitelson and Merzlyak (1994)
SIPI	Structure insensitive pigment index	$\frac{\rho_{780}-\rho_{440}}{\rho_{780}-\rho_{670}}$ (9)	Penuelas et al. (1995)
GNDVI	Green Normalized Difference Vegetation Index	$\frac{\rho_{780}-\rho_{550}}{\rho_{780}+\rho_{550}}$ (10)	Gitelson et al. (1996)
OSAVI	Optimized Soil Adjusted Vegetation Index	$(1+0.16)\frac{(\rho_{780}-\rho_{670})}{(\rho_{780}+\rho_{670}+0.16)}$ (11)	Rondeaux et al. (1996)
TVI	Triangular Vegetation Index	$0.5\left[(670-550)(\rho_{780}-\rho_{550})-(780-550)(\rho_{670}-\rho_{550})\right]$ (12)	Broge and Leblanc (2000)
TCARI	Transformed chlorophyll absorption reflectance index	$3\left[(\rho_{700}-\rho_{670})-0.2(\rho_{700}-\rho_{550})\left(\frac{\rho_{700}}{\rho_{670}}\right)\right]$ (13)	Haboudane et al. (2002)
TGI	Triangular greenness index	$-0.5\left[(670-490)(\rho_{670}-\rho_{550})-(670-550)(\rho_{670}-\rho_{490})\right]$ (14)	Hunt et al. (2011)

The band centers/band widths used to calculate these vegetation indices differ slightly from those used by the referenced publications. In all cases, the MiniMCA12 bands closest in center wavelength to the original indices were used as substitutes. The symbol ρ indicates the relative reflectance of the subscripted wavelength in nm

A PLS-R yield validation model for grain and ear weight was obtained for each of the five post treatment development stages (V10, V12, VT, R2 and R4) using the 11 Mini-iMCA12 bands from each associated date (Table 3, Fig. 3). The R2 development stage had the grain yield validation model with highest R^2 and the lowest RMSEV values, as well as the validation model with the highest R^2 value for ear weight. The VT development stage had the validation model with the lowest RMSEV value for ear weight. Here then, the R2 development stage appears to be best for predicting maize yield. In contrast, Ma et al. (1996) showed that maize grain yield and NDVI based on canopy reflectance may also be well correlated (correlation coefficient (r) = 0.81) using reflectance during the vegetative development stages at two weeks pre-anthesis assumed to be V10. Geipel et al. (2014) achieved even better maize grain yield predictions with validation R^2 values peaking at 0.74 and RMSEV values ranging from 0.67 to 1.28 t/ha. The latest development stage analyzed was the complete ear emergence (refered to as developmnet stage Z58; Zadoks et al., 1974) that is just before VT. Thomason et al. (2007) explored grain yield prediction for V6–V9 and V11–V14 development stages and presented R^2 values of 0.65 and 0.34, respectively, though did not report RMSE. Inman et al. (2007) used an active spectral sensor for yield assessment and achieved their highest R^2 value of 0.76 for the V6–V8 development stages. Vergara-Diaz et al. (2016) applied RGB indices based on ground level imagery to correlate maize grain yield with the VT development stage and resulted with a nonlinear correlation with an R^2 value of 0.72, though no yield prediction was presented. An early yield prediction may miss important effects on yield that occur during the reproductive stages. For example, drought stressed maize during the reproductive development stages can reduce yield while stress during early vegetative stages reduces growth but may not greatly reduce yield (Mansouri-Far et al. 2010). Thus, assessment at early reproductive stages is likely more practical.

The current study compares favorably to studies predicting maize yield from spectral data. Shanahan et al. (2001) presented r values of approximately 0.80 for their correlations of VIs with maize grain yield. They achieved a maximum r value of 0.95 for a relatively late reproductive development stage (21 days after R3), though did not presented any yield predictions. Farrell et al. (2018) also examined VIs correlation with maize grain yield for the flowering development stage and presented r value of 0.88, though no yield prediction was presented. Zaman-Allah et al. (2015) explored the correlation of spectral imagery from UAV to maize grain yield for the R1 development stage. They found a maximal coefficient of correlation value of −0.74 for the crop senescence index and the entire range of grain yield (1.9–8.6 t/ha), and 0.72 using NDVI for a grain yield range of 1.9–4.6 t/ha. Weber et al. (2012) showed a grain yield prediction with an $R^2 = 0.69$ with rRMSE of 16 t/ha for the R1–R3 development stages by hyperspectral canopy data accessed from ground level. In the current study, for similar development stages, grain yield was predicted by a validation model with an R^2 value of 0.73 and rRMSE value of 7.79 (Table 3). The models developed in the current study are for full and deficit irrigation together (allowing a relatively wide range of traits values) similar to the data analyzed by the above mentioned model of Weber et al. (2012). It is assumed that acquiring hyperspectral aerial imagery of maize under full and deficit irrigation treatments would result in an improved grain yield assessment.

The best grain yield and ear weight validation models had RMSEV values of 2.07 and 3.41 t/ha, respectively (Table 3). These predication values are for the entire range of measured yields (grain and ear), and it is likely that this wide range of yield (which is a consequence of including both deficit and full irrigation treatments; Fig. 2) contributed to the relatively high R^2 values of the models. However, this RMSEV reiterates that the

Table 3 Results of partial least squares regression (PLS-R) models to predict grain yield and ear weight from superspectral aerial images at different developmental stages

	Development stages[a]														
	V10			V12			VT			R2			R4		
	R^2	RMSE	rRMSE	R^2	RMSE	rRMSE	R^2	RMSE	rRMSE	R^2	RMSE	rRMSE	R^2	RMSE	rRMSE
Grain yield (t/ha)															
Calibration	0.60	2.62	7.67	0.68	2.38	6.97	0.67	2.42	7.08	0.77	2.08	6.09	0.73	2.10	6.14
Cross validation	0.52	2.90	8.49	0.60	2.69	7.87	0.60	2.68	7.85	0.70	2.37	6.94	0.70	2.22	6.50
Validation	0.58	2.84	8.31	0.57	2.72	7.96	0.61	2.58	7.55	0.73	2.07	6.06	0.65	2.66	7.79
Ears weight (t/ha)															
Calibration	0.31	3.94	9.96	0.51	3.47	8.77	0.41	3.90	9.86	0.54	3.31	8.37	0.51	3.26	8.24
Cross validation	0.27	4.07	10.29	0.43	3.74	9.45	0.38	4.02	10.16	0.49	3.50	8.85	0.46	3.41	8.62
Validation	0.23	4.44	11.23	0.46	3.42	8.65	0.38	3.37	8.52	0.49	3.41	8.62	0.48	3.84	9.71

	All dates of measured property											
	CC (%)				RWC (%)				LAI			
	R^2	RMSE	rRMSE	# of samples	R^2	RMSE	rRMSE	# of samples	R^2	RMSE	rRMSE	# of samples
Calibration	0.86	9.94	25.62	502	0.58	5.25	5.38	314	0.84	0.86	10.55	502
Cross validation	0.85	10.10	26.03	502	0.56	5.40	5.53	314	0.84	0.88	10.80	502
Validation	0.86	9.56	24.64	215	0.55	5.65	5.79	135	0.85	0.86	10.55	214

Calibration and cross validating datasets of the grain yield and the ear weight included 106 samples and the validation dataset included 45 samples. The leaf area index (LAI), relative water content (RWC) and canopy cover (CC) PLS-R models were applied for all dates in which a given trait was obtained (Table 1). All R2 are significant, with $p < 0.01$

[a]Maize development stages are divided into vegetative (V) and reproductive (R) categories, separated by the vegetative tasseling (VT) stage

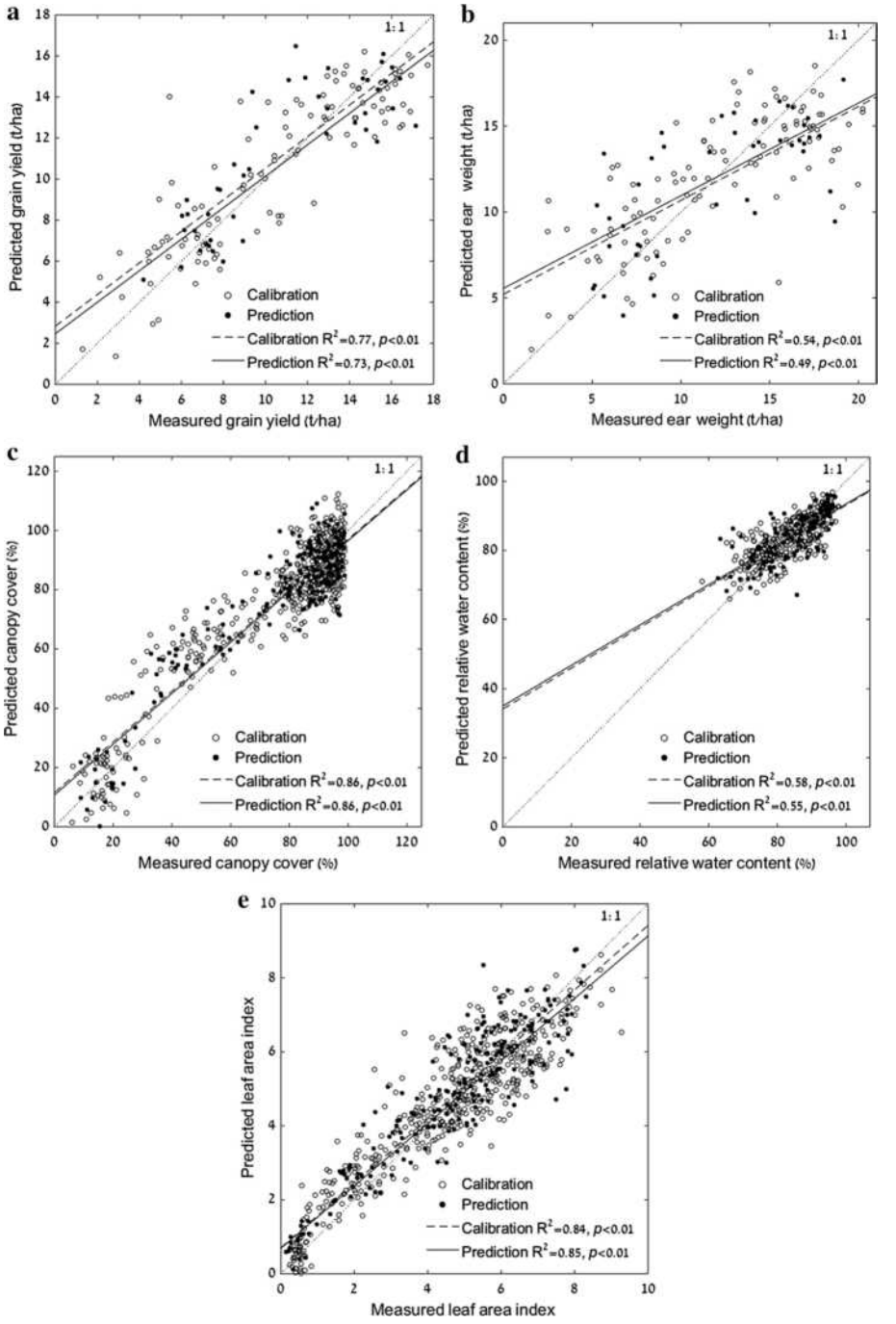

Fig. 3 Predicted versus measured traits from partial least squares regression (PLS-R) models: **a** maize grain yield, **b** ear weight, **c** canopy cover (CC), **d** relative water content (RWC), and **e** Leaf Area Index (LAI)

models are more sensitive to within yield variation at lower rather than higher overall yields.

In addition to yield, superspectral data PLS-R models also well predicted CC, RWC and LAI (Table 3, Fig. 3). The ability to predict maize yield using PLS-R derives from the sensitivity of the spectral data to the broad set of foliar properties that drive yield (Weber et al. 2012). The yield prediction from the superspectral imagery may therefore be due in part to relationships between yield and canopy properties (i.e., more vigorous canopies produce higher yields), and indeed yields are often tied to foliar properties such as CC, LAI and RWC (Weber et al. 2012; Araus et al. 2012). However, the results show only modest correlations between yield and the three foliar traits (Table 4). In fact, the ability to predict yield as a function of CC declines with developmental stage, suggesting that as plants develop, the ability to predict yield spectrally is a function of a wide range of foliar attributes, not just CC. This is further supported by an evaluation of the PLS-R coefficients for predicting each trait (Fig. 4), which differ considerably between yield and the canopy traits CC, RWC and LAI.

Yield assessment by vegetation indices

Vegetation indices are widely used for agronomic assessments because of their ease of implementation, but typically do not perform as well as PLS-R models, as confirmed in Table 5 showing correlation to yield for V10, V12, VT, R2, and R4 with 14 vegetation indices and Table 6 showing validation for the 10 best VI models. Notably, the red-edge inflection point (REIP) and normalized difference red-edge index (NDREI) indices, based on red-edge bands, were effective to estimate grain and ear yield in multiple cases, including for V12, R2 and R4. The importance of the red-edge for spectral yield estimation was revealed by the PLS-R coefficients of the 740 nm and 780 nm bands (Fig. 4). Also of note, none of the best predictive models occurred at VT, likely because the tassel has a spectral signature that is distinctively different from leaf spectra (Vina et al. 2004), thus partly obscuring spectral canopy properties important to estimating yield. PLS-R grain yield validation models (Table 3) were of a similar quality for the VT and V12 development stages, illustrating the advantage of using all bands instead of VIs.

PLS-DA spectral classification models

Phenology by spectral classification

Crop management can benefit from being able to map developmental stages (Nguy-Robertson et al. 2013), especially on large fields in which multiple varieties bred for different traits are present. Spectrally identifying development stage from a UAV can be useful to determine the current development stage of the field (or part of it) and apply the appropriate yield prediction model. Spectral data obtained from the UAV (canopy level) and from the field spectrometer (leaf level) resulted in high quality separation between development stages per irrigation treatment (Table 7), although the PLS-DA did not perform well when the two irrigation treatments were combined (results not shown). This presents some challenges in application since plant water availability, and therefore status, may be heterogeneous in a field. To address this, PLS-DA was also used to distinguish treatments per developmental stage. For the superspectral PLS-DA full irrigation model, the VIP statistic indicates that the most important bands for discrimination of growth stages

Table 4 Correlation coefficient (r) values between grain yield and ear weight and traits

Development stage[a]	Grain yield (t/ha)			Ear weight (t/ha)		
	CC	RWC	LAI	CC	RWC	LAI
V10	0.17	0.08	0.17	0.10	0.07	0.12
V12	0.08	–	0.14	0.08	–	0.10
VT	0.02^{ns}	0.04	0.01^{ns}	0.01^{ns}	0.03	0.00^{ns}
R2	–	–	–	–	–	–
R4	0.00^{ns}	0.11	0.02^{ns}	0.00^{ns}	0.04	0.01^{ns}

Canopy cover (CC), relative water content (RWC) and leaf area index (LAI). All r values are significant to $p < 0.05$ unless ns (not significant) is noted

[a]Maize development stages are divided into vegetative (V) and reproductive (R) categories, separated by the vegetative tasseling (VT) stage

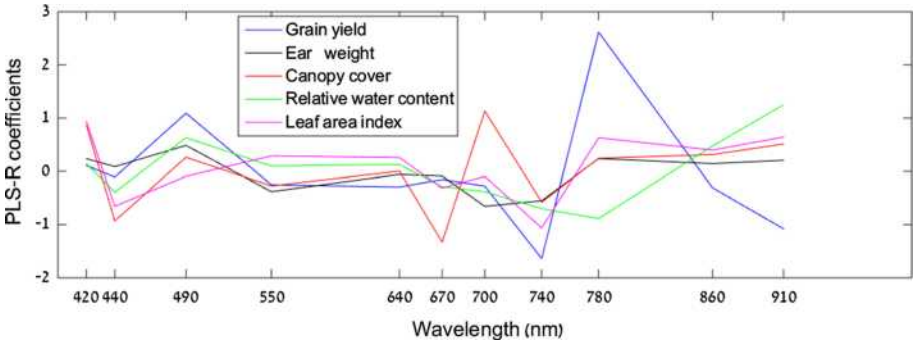

Fig. 4 The partial least squares regression (PLS-R) coefficients for all five of the trait models shown in Fig. 3. A color version of the figure is available on-line

Table 5 Correlation coefficient (r) values of grain yield and ear weight by vegetation indices in five development stages

Index	Grain yield					Ear weight				
	V10[a]	V12[a]	VT[a]	R2[a]	R4[a]	V10[a]	V12[ba]	VT[a]	R2[a]	R4[a]
SR	0.67	0.43	0.71	0.21	0.80	0.56	0.33	0.60	0.19[ns]	0.69
NDVI	0.62	0.43	0.69	0.21	0.77	0.52	0.33	0.60	0.20[ns]	0.68
NGRDI	0.73	0.05[ns]	0.51	−0.49	0.40	0.61	0.03[ns]	0.43	−0.45	0.35
REIP	−0.30	0.76	0.50	0.78	0.79	−0.23	0.68	0.49	0.70	0.70
RARSa	−0.65	0.23	−0.44	0.56	−0.14[ns]	−0.57	0.27	−0.36	0.54	−0.14[ns]
RARSb	−0.49	−0.38	−0.60	−0.48	−0.62	−0.45	−0.45	−0.59	−0.51	−0.57
RARSc	0.50	0.32	0.65	−0.04[ns]	0.72	0.41	0.24	0.56	0.02[ns]	0.61
NDREI	0.00 [ns]	0.76	0.57	0.79	0.81	0.04[ns]	0.68	0.55	0.70	0.72
SIPI	−0.61	−0.32	−0.64	−0.23	−0.74	−0.51	−0.23	−0.54	−0.21	−0.66
GNDVI	0.25	0.57	0.71	0.53	0.80	0.21	0.45	0.62	0.49	0.70
OSAVI	0.63	0.30	0.61	−0.10[ns]	0.75	0.50	0.17[ns]	0.49	−0.15[ns]	0.65
TVI	0.61	0.20[ns]	0.44	−0.23	0.63	0.47	0.06[ns]	0.32	−0.28	0.53
TCARI	0.64	−0.29	0.08[ns]	−0.55	−0.23	0.53	−0.34	0.00[ns]	−0.55	−0.20[ns]
TGI	0.68	−0.27	−0.01[ns]	−0.57	−0.28	0.53	−0.31	−0.07[ns]	−0.55	−0.27

All r values are significant to $p < 0.01$ unless ns (not significant) is noted

[a]Maize development stages are divided into vegetative (V) and reproductive (R) categories, separated by the vegetative tasseling (VT) stage

were the blue, red-edge and NIR (Fig. 5a), while for the deficit irrigation the most important bands were the blue and red-edge bands (Fig. 5b) and less so the NIR. For the VT stage the most important band was in the visible range, likely due to the presence of tassels (Vina et al. 2004). The V4 stage showed similar importance of bands for both the full and deficit irrigation treatments (Fig. 5a, b), assumed to be a result of relatively high portion of soil background. Different bands are important for full and deficit irrigation at the V6 stage, illustrating that by V6 the irrigation treatment has a stronger impact on green reflectance than the soil background. The VIP trend of the VT stage looks the same for both

Table 6 The top ten predictions for both yield grain and ear weight are presented based on the 14 vegetation indices and five development stages

Development stage[a]	Vegetation indices	R^2_{cal}	RMSEC	rRMSEC	R^2_{val}	RMSEV	rRMSEV
Grain yield (t/ha)							
R4	NDREI	0.68	2.36	6.91	0.61	2.71	7.95
R4	GNDVI	0.67	2.41	7.06	0.59	2.79	8.18
R2	NDREI	0.65	2.46	7.19	0.56	2.88	8.44
R4	REIP	0.65	2.46	7.20	0.56	2.88	8.42
R2	REIP	0.64	2.51	7.34	0.56	2.89	8.45
R4	SR	0.63	2.53	7.40	0.65	2.58	7.55
R4	NDVI	0.60	2.66	7.77	0.57	2.85	8.36
V12	NDREI	0.56	2.76	8.09	0.59	2.77	8.11
R4	SIPI	0.56	2.77	8.10	0.54	2.95	8.62
V12	REIP	0.56	2.77	8.10	0.59	2.78	8.15
Ear weight (t/ha)							
R4	NDREI	0.53	3.27	8.27	0.47	3.76	9.50
R2	NDREI	0.53	3.29	8.33	0.43	3.90	9.87
R4	GNDVI	0.52	3.31	8.36	0.44	3.86	9.75
R2	REIP	0.51	3.33	8.43	0.44	3.86	9.75
R4	REIP	0.50	3.37	8.51	0.44	3.87	9.78
R4	SR	0.50	3.37	8.52	0.44	3.87	9.80
R4	NDVI	0.48	3.44	8.69	0.41	3.98	10.06
V12	REIP	0.47	3.49	8.83	0.44	3.88	9.80
V12	NDREI	0.47	3.49	8.83	0.44	3.88	9.81
R4	SIPI	0.46	3.52	8.91	0.40	4.02	10.16

All R2 values are significant to $p < 0.01$. The full table with all predictions may be found in supplementary data table S1

[a]Maize development stages are divided into vegetative (V) and reproductive (R) categories, separated by the vegetative tasseling (VT) stage

irrigation treatments and shows the influence of the tassels. For the hyperspectral PLS-DA models the most important spectral regions are the visible, red-edge, and the water absorption regions around 1400 and 1900 nm (Fig. 5c, d). For the PLS-DA full irrigation treatment, two important spectral regions occur around 1640 nm and 2160 nm that are related to lignin (Ben-Dor et al. 1997; Curran 1989) and changes in lignin concentration across plant development stages (Frei 2013). These lignin related wavelengths are relatively less important for the deficit irrigation treatment as water absorption features are relatively more important in the classification model.

Treatment by spectral classification

Irrigation treatments were classified by PLS-DA for superspectral and hyperspectral data of all 151 plots with 19 hybrids and 40 plots with 5 hybrids, respectively (Table 8). All total accuracies are higher than 87% and showed a high ability to classify the irrigation treatments. The R2 development stage is the most appropriate for yield assessment and has shown the highest accuracies for the superspectral model. The VIP trend of

Table 7 Partial least squares discriminant analysis (PLS-DA) total accuracies and Cohen's Kappa are given by irrigation treatment

Classes	Treatment	Calibration (Kappa)	Cross validation (Kappa)	Validation (Kappa)
Superspectral airborne data—19 varieties				
Two development stages[a]	Deficit irrigation	100 (1)	100 (1)	100 (1)
Two development stages[a]	Full irrigation	100 (1)	100 (1)	100 (1)
Seven development stages[b]	Deficit irrigation	91.6 (0.90)	87.9 (0.86)	90.9 (0.89)
Seven development stages[b]	Full irrigation	97.6 (0.97)	96.7 (0.96)	96.3 (0.96)
Hyperspectral ground level data—five varieties				
Two development stages[a]	Deficit irrigation	100 (1)	100 (1)	91.7 (0.83)
Two development stages[a]	Full irrigation	100 (1)	96.4 (0.93)	100 (1)
Five development stages[c]	Deficit irrigation	94.2 (0.93)	91.3 (0.89)	90 (0.88)
Five development stages[c]	Full irrigation	94.4 (0.93)	88.7 (0.86)	93.3 (0.92)

Each calibration model was cross-validated during model calibration and tested (validation column) on samples withheld from the calibration and cross validation

[a]V10 and R4; [b]V4, V6, V10, V12, VT, R2 and R4; [c]V6, V10, VT, R2 and R4

the R2 development stage (Fig. 6a) shows importance for the red-edge. The red-edge is related to several traits that can be generally defined as plant health or vigor (Horler et al. 1983; Herrmann et al. 2011; Baret et al. 1992). The red-edge is also important to the V12 development stage model and it can be assumed that without the tassel effect (Vina et al. 2004) it would be the same for the VT stage. Notably, 2 days prior to superspectral data acquisition of the R2 stage the deficit irrigation treatment was irrigated (Table 1). Because the red-edge is related to the "blue shift" associated with water stress (Wang et al. 2007), it was assumed that the relationship held because plants under deficit irrigation had not fully recovered because chlorophyll full recovery takes more than 2 days (Sanchez et al. 1983).

The model for the R4 stage showed the importance of the red and NIR bands as a result of leaf senescence influencing canopy structure in the deficit irrigation treatment (Gausman 1985). In Fig. 6b, the irrigation treatments are classified by each of the growth stages, therefore, the VIP results in peaks less uniform than in Fig. 5c and d. The visible spectral range showed importance only for R2 and R4, both with the same peaks at 570 and 620 nm. Tattini et al. (2004) has shown that flavonoids fluoresce at 570 nm after drought stress. Melanins in fungi spectrally absorb in 570 and 620 nm (Almendros 2008). Both, melanins and flavonoids are antioxidant pigments with phenol compounds (Carletti et al. 2014). Flavonoid production is enhanced after ultra violet exposure (Carletti et al. 2014) and influenced by drought stress (Avramova et al. 2015). This may explain the importance of VIP peaks at 570 and 620 nm for R2 and R4 in the irrigation treatments. The VIP in the water bands around 1400 and 1900 nm do not peak as in Fig. 5b and d, suggesting that water stress (detectable from the visible) is more important to these PLS-DA models than water content. There are many VIP peaks in the short wave infrared region, for example, the 1010 nm peak in the VT and 1460 nm peak in R2 and R4 both of lignin, as well as peaks at 1530, 1770, 1900, 1960, 2000, 2080, 2260 and 2320 nm that are related to starch content (Curran 1989). Lignin and starch are both influenced by water stress (Barnaby et al. 2013; Le Gal et al. 2015).

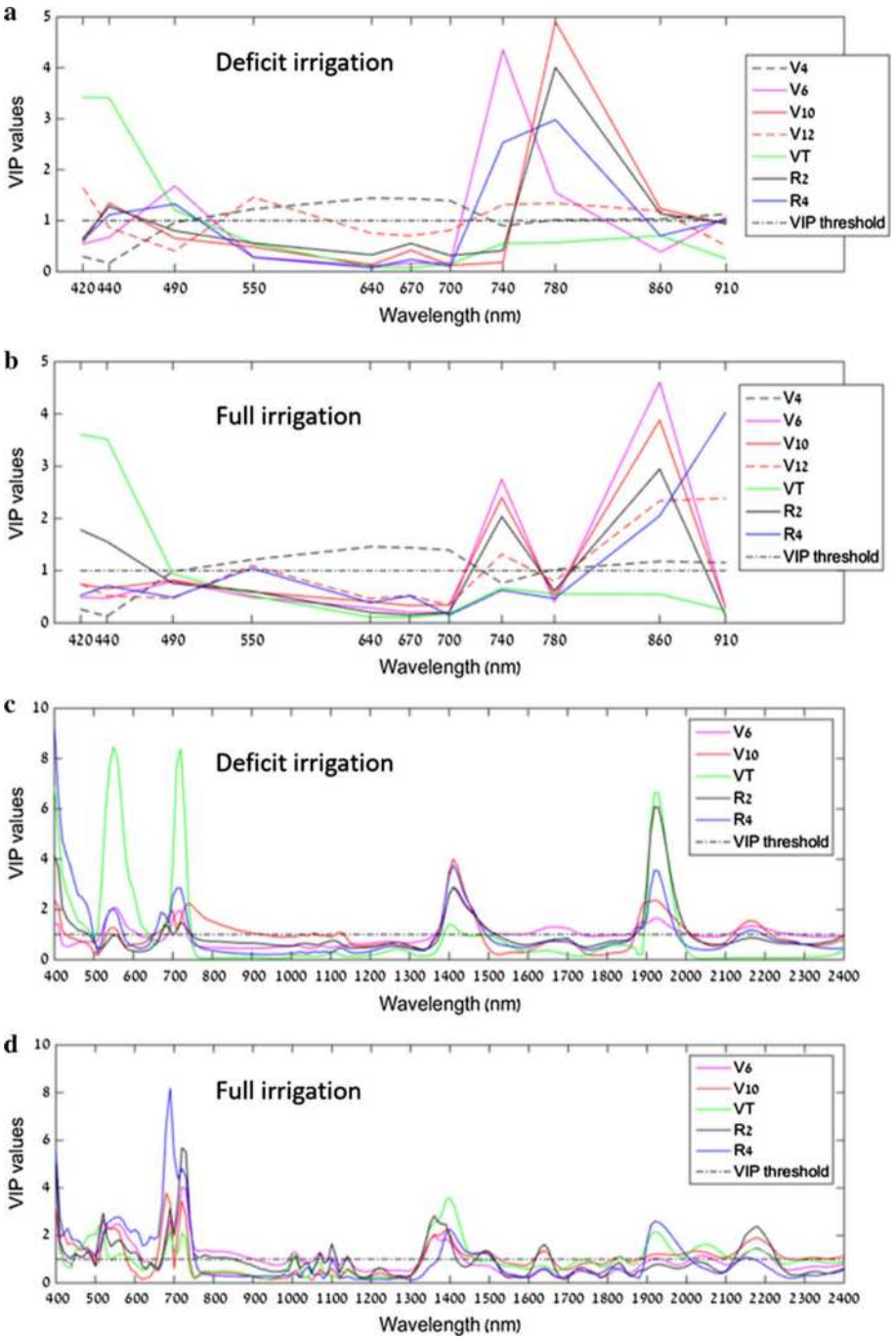

Fig. 5 The variable importance in projection (VIP) values for the seven- and five- development stage models presented in Table 7: **a** and **b** for superspectral models and **c** and **d** for hyperspectral models. A color version of the figure is available on-line

Table 8 Partial least squares discriminant analysis (PLS-DA) accuracies for identifying irrigation treatment of given development stages using airborne superspectral as well as ground level, leaf contact hyperspectral data

	Superspectral airborne data—19 varieties			Hyperspectral ground level data—five varieties		
Development stage[a]	Calibration (Kappa)	Cross validation (Kappa)	Validation (Kappa)	Calibration (Kappa)	Cross validation (Kappa)	Validation (Kappa)
V10	94.3 (0.89)	93.1 (0.87)	91.1 (0.82)	100 (1)	91.9 (0.84)	91.6 (0.83)
V12	94.3 (0.89)	93.4 (0.88)	93.3 (0.87)	–	–	–
VT	97.2 (0.94)	92.4 (0.85)	93.3 (0.87)	100 (1)	87.2 (0.75)	91.6 (0.83)
R2	100 (1)	100 (1)	97.7 (0.96)	100 (1)	99.1 (0.98)	95.8 (0.92)
R4	97.2 (0.94)	97.2 (0.94)	97.7 (0.96)	100 (1)	97.3 (0.95)	97.9 (0.96)

[a]Maize development stages are divided into vegetative (V) and reproductive (R) categories, separated by the vegetative tasseling (VT) stage

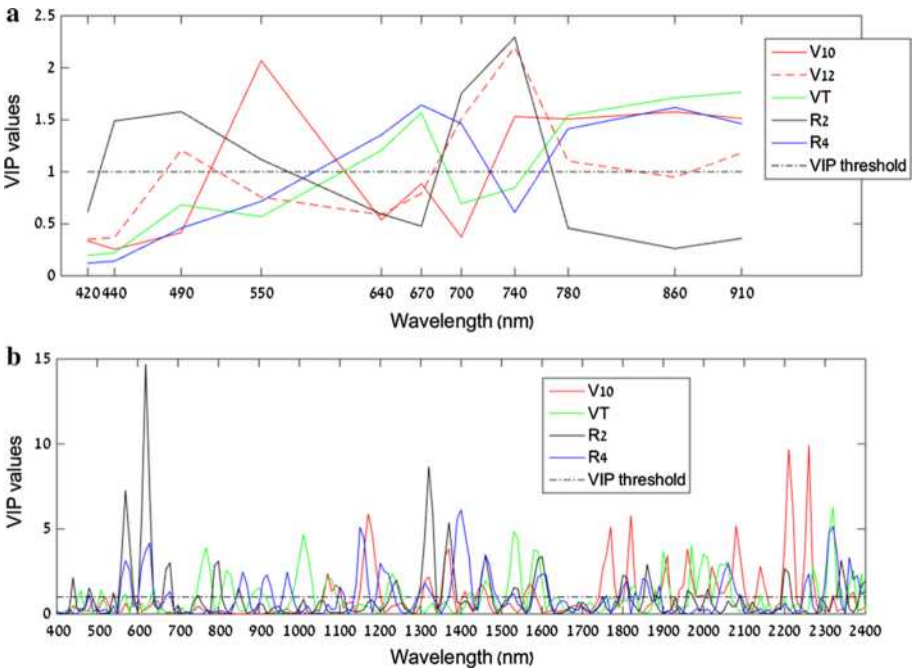

Fig. 6 The variable importance in projection (VIP) values of the irrigation treatment models presented in Table 8: **a** for superspectral data and **b** for hyperspectral data. A color version of the figure is available online

The ability to spectrally distinguish between irrigation treatments as well as between development stages allow detection of irrigation status and phenology. Thus, yield prediction analysis steps are suggested for a field with known or unknown development stage (Fig. 7).

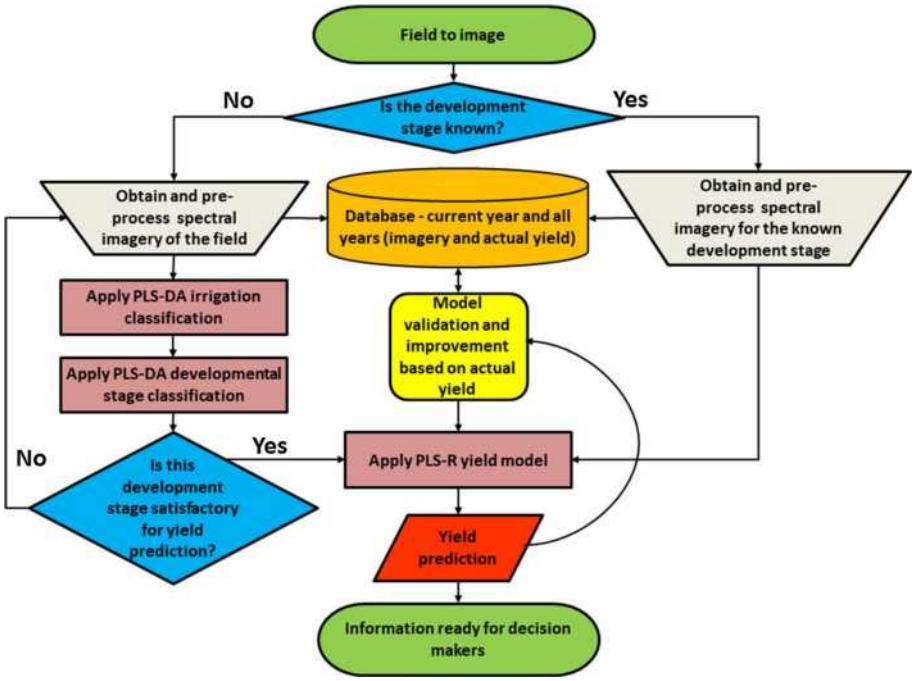

Fig. 7 Yield prediction analysis steps for a field with either a known or unknown development stage when spectral data are obtained

Summary and conclusions

The current study used superspectral airborne imagery to predict maize grain yield and ear weight, and to discriminate among growth stages and irrigation treatments. Models for grain yield and ear weight were developed for each of the five development stages. The deficit and full irrigation treatments were spectrally identified, as well as the development stages for each of those treatments. In practical application, once the development stage of the field is identified, the relevant yield prediction model can be implemented. In practice, yield prediction models can be validated and improved, based on site specific yield data obtained while harvesting. The main conclusions can be summarized as:

- Development stage R2 was found to be the best stage for applying yield prediction using PLS-R.
- Vegetation indices can predict grain yield as well as ear weight but in most cases with lower predictive accuracy than the PLS-R models.
- The red-edge region is involved in most of the vegetation indices that resulted in the highest R^2 calibration values for grain yield as well as ear weight. The red-edge bands show the highest importance for grain yield prediction by PLS-R models.
- PLS-DA classification models can spectrally separate maize development stages based on canopy (superspectral resolution from UAV) and leaf (hyperspectral resolution on ground) for both irrigation treatments.

- PLS-DA classification models can spectrally separate maize irrigation treatments based on canopy (superspectral resolution from UAV) and leaf (hyperspectral resolution on ground) for development stages.

The yield prediction models and analysis steps can be tested in commercial fields from UAV or scaled up to imagery from the VENμS satellite. It might be that scaling up from approximately 12 m^2 plots explored in the current study to the 25 m^2 satellite pixels will require modifications to the statistical models.

Acknowledgments This research was supported by the Israeli Ministry of Agriculture and Rural Development (Eugene Kandel Knowledge Centers) as part of the Root of the Matter - The root zone knowledge center for leveraging modern agriculture (Contract No. 16-34-0005). The postdoctoral Pratt foundation partially supported Ittai Herrmann. The Townsend lab received support from USDA Hatch funding (Project WIS01874). The authors would like to thank: Alexander Goldberg for all his help in the field and much beyond; Offir Matsrafi for his long term and long distance GIS support; Michael Travis from the University of Wisconsin-Extension, Pepin County for sharing his knowhow regarding corn cultivation in the Midwest; Aditya Singh for his insights; Ben Spaier for his comments, questions and proofreading; Evogene Ltd.: agronomist Mor Manor and his team; phenotyping team, led by Raanan Ganor; sampling team, led by Sara Koretzki; data and imaging team, led by Yogev Montekyo; and R&D Researchers that helped and supported planning and management, especially Inbal Dangoor, Ronit Rimon Knopf and Alon Glick.

Compliance with ethical standards

Conflict of interest The authors declare that they have no conflict of interest.

References

Adao, T., Hruska, J., Padua, L., Bessa, J., Peres, E., Morais, R., et al. (2017). Hyperspectral Imaging: A review on UAV-based sensors, data processing and applications for agriculture and forestry. *Remote Sensing*. https://doi.org/10.3390/rs9111110.

Akins, M. S., & Shaver, R. D. (2014). Effect of corn snaplage on lactation performance by dairy cows. *The Proffecional Animal Scientist, 30,* 86–92.

Almendros, G. M. (2008). Humic substances. In W. Cheswarth (Ed.), *Encyclopedia of soil science* (pp. 315–323). Dordrecht, The Netherlands: Springer.

Andrade-Sanchez, P., Gore, M. A., Heun, J. T., Thorp, K. R., Carmo-Silva, A. E., French, A. N., et al. (2014). Development and evaluation of a field-based high-throughput phenotyping platform. *Functional Plant Biology, 41*(1), 68–79. https://doi.org/10.1071/fp13126.

Araus, J. L., Serret, M. D., & Edmeades, G. O. (2012). Phenotyping maize for adaptation to drought. *Frontiers in Physiology*. https://doi.org/10.3389/fphys.2012.00305.

Avramova, V., AbdElgawad, H., Zhang, Z. F., Fotschki, B., Casadevall, R., Vergauwen, L., et al. (2015). Drought induces distinct growth response, protection, and recovery mechanisms in the maize leaf growth zone. *Plant Physiology, 169*(2), 1382–1396. https://doi.org/10.1104/pp.15.00276.

Baret, F., Jacquemoud, S., Guyot, G., & Leprieur, C. (1992). Modeled analysis of the biophysical nature of spectral shifts and comparison with information-content of broad bands. *Remote Sensing of Environment, 41*(2–3), 133–142.

Barnaby, J. Y., Kim, M., Bauchan, G., Bunce, J., Reddy, V., & Sicher, R. C. (2013). Drought responses of foliar metabolites in three maize hybrids differing in water stress tolerance. *PLoS ONE*. https://doi.org/10.1371/journal.pone.0077145.

Barrett, J. P. (1974). Coefficient of determination—Some limitations. *American Statistician, 28*(1), 19–20. https://doi.org/10.2307/2683523.

Barrs, H. D., & Weatherley, P. E. (1962). A re-examination of the relative turgidity technique for estimating water deficits in leaves. *Australian Journal of Biological Sciences, 15*(3), 413–428.

Ben-Dor, E., Inbar, Y., & Chen, Y. (1997). The reflectance spectra of organic matter in the visible near-infrared and short wave infrared region (400–2500 nm) during a controlled decomposition process. *Remote Sensing of Environment, 61*(1), 1–15. https://doi.org/10.1016/s0034-4257(96)00120-4.

Broge, N. H., & Leblanc, E. (2000). Comparing prediction power and stability of broadband and hyperspectral vegetation indices for estimation of green leaf area index and canopy chlorophyll density. *Remote Sensing of Environment, 76*(2), 156–172.

Burkart, A., Hecht, V. L., Kraska, T., & Rascher, U. (2018). Phenological analysis of unmanned aerial vehicle based time series of barley imagery with high temporal resolution. *Precision Agriculture, 19*(1), 134–146. https://doi.org/10.1007/s11119-017-9504-y.

Carletti, G., Nervo, G., & Cattivelli, L. (2014). Flavonoids and Melanins: A common strategy across two kingdoms. *International Journal of Biological Sciences, 10*(10), 1159–1170. https://doi.org/10.7150/ijbs.9672.

Chappelle, E. W., Kim, M. S., & McMurtrey, J. E. (1992). Ratio analysis of reflectance spectra (RARS): an algorithm for the remote estimation of the concentrations of chlorophyll a, chlorophyll b, and carotenoids in soybean leaves. *Remote Sensing of Environment, 39*(3), 239–247. https://doi.org/10.1016/0034-4257(92)90089-3.

Cohen, J. (1960). A coefficient of agreement for nominal scales. *Educational and Psychological Measurement, 20*(1), 37–46.

Colomina, I., & Molina, P. (2014). Unmanned aerial systems for photogrammetry and remote sensing: A review. *Isprs Journal of Photogrammetry and Remote Sensing, 92,* 79–97. https://doi.org/10.1016/j.isprsjprs.2014.02.013.

Curran, P. (1989). Remote sensing of foliar chemistry. *Remote Sensing of the Environment, 30,* 271–278.

Darby, H., & Lauer, J. (2006). Critical stages in the life of a corn plant. Retrieved July 8, 2017, from http://corn.agronomy.wisc.edu/Management/pdfs/CriticalStages.pdf.

Decagon Devices, I. (2016). AccuPAR PAR/LAI ceptometer, model LP-80. Operator's manual. WA, USA: Pullman.

Duvick, D. N. (2005). Genetic progress in yield of united states maize. *Maydica, 50*(3–4), 193–202.

FAO (2016) 'Crops world wide area harvested and production' Fao. Retrieved April 27, 2018, from http://www.fao.org/faostat/en/#data/QC.

Farrell, M., Gili, A., & Noellemeyer, E. (2018). Spectral indices from aerial images and their relationship with properties of a corn crop (journal article). *Precision Agriculture*. https://doi.org/10.1007/s11119-018-9570-9.

Ferraretto, L. F., Shaver, R. D., & Luck, B. D. (2018). Silage review: Recent advances and future technologies for whole-plant and fractionated corn silage harvesting. *Journal of Dairy Science, 101*(5), 3937–3951. https://doi.org/10.3168/jds.2017-13728.

Ferrio, J. P., Villegas, D., Zarco, J., Aparicio, N., Araus, J. L., & Royo, C. (2005). Assessment of durum wheat yield using visible and near-infrared reflectance spectra of canopies. *Field Crops Research, 94*(2–3), 126–148. https://doi.org/10.1016/j.fcr.2004.12.002.

Frei, M. (2013). Lignin: Characterization of a multifaceted crop component. *Sci World J, 13,* 436517. https://doi.org/10.1155/2013/436517.

Gausman, H. (1985). *Plant leaf optical properties in visible and Near Infrared light*. Lubbock TX, USA: Texas Tech Press.

Geipel, J., Link, J., & Claupein, W. (2014). Combined spectral and spatial modeling of corn yield based on aerial images and crop surface models acquired with an unmanned aircraft system. *Remote Sensing, 6*(11), 10335–10355. https://doi.org/10.3390/rs61110335.

Gitelson, A. A., Kaufman, Y. J., & Merzlyak, M. N. (1996). Use of a green channel in remote sensing of global vegetation from EOS-MODIS. *Remote Sensing of Environment, 58*(3), 289–298.

Gitelson, A., & Merzlyak, M. N. (1994). Quantitative estimation of chlorophyll-a using reflectance spectra: Experiments with autumn chestnut and maple leaves. *Journal of Photochemistry and Photobiology B-Biology, 22*(3), 247–252. https://doi.org/10.1016/1011-1344(93)06963-4.

Gore, M. A., Chia, J. M., Elshire, R. J., Sun, Q., Ersoz, E. S., Hurwitz, B. L., et al. (2009). A first-generation haplotype map of maize. *Science, 326*(5956), 1115–1117. https://doi.org/10.1126/science.1177837.

Guyot, G., & Baret, F. (1988). Utilisation de la haute resolution spectrale pour suivre l'etat des couverts vegetaux. Esa *4th International Colloquium "Spectral signatures of objects in remote sensing"*. 18–22 January. Aussois: Paris: ESA pablication, pp. 279–286.

Haboudane, D., Miller, J. R., Tremblay, N., Zarco-Tejada, P. J., & Dextraze, L. (2002). Integrated narrow-band vegetation indices for prediction of crop chlorophyll content for application to precision agriculture. *Remote Sensing of Environment, 81*(2–3), 416–426.

Hansen, P. M., & Schjoerring, J. K. (2003). Reflectance measurement of canopy biomass and nitrogen status in wheat crops using normalized difference vegetation indices and partial least squares regression. *Remote Sensing of Environment, 86,* 542–553.

Herrmann, I., Pimstein, A., Karnieli, A., Cohen, Y., Alchanatis, V., & bonfil, D. (2011). LAI assessment of wheat and potato crops by VENμS and Sentinel-2 bands. *Remote Sensing of Environment, 115,* 2141–2151.

Horler, D. N. H., Dockray, M., & Barber, J. (1983). The red edge of plant leaf reflectance. *International Journal of Remote Sensing, 4*(2), 273–288.

Hunt, E. R., Jr., Daughtry, C. S. T., Eitel, J. U. H., & Long, D. S. (2011). Remote sensing leaf chlorophyll content using a Visible Band Index. *Agronomy Journal, 103*(4), 1090–1099. https://doi.org/10.2134/agronj2010.0395.

Inman, D., Khosla, R., Reich, R. M., & Westfall, D. G. (2007). Active remote sensing and grain yield in irrigated maize. *Precision Agriculture, 8*(4–5), 241–252.

Jetz, W., Cavender-Bares, J., Pavlick, R., Schimel, D., Davis, F. W., Asner, G. P., et al. (2016). Monitoring plant functional diversity from space. *Nature Plants*. https://doi.org/10.1038/nplants.2016.24.

Jordan, C. F. (1969). Derivation of leaf area index from quality of light on the forest floor. *Ecology, 50*(4), 663–670. https://doi.org/10.2307/1936256.

Kirchgessner, N., Liebisch, F., Yu, K., Pfeifer, J., Friedli, M., Hund, A., et al. (2016). The ETH field phenotyping platform FIP: a cable-suspended multi-sensor system. *Functional Plant Biology, 44*(1), 154–168.

Laliberte, A. S., Goforth, M. A., Steele, C. M., & Rango, A. (2011). Multispectral remote sensing from unmanned aircraft: Image processing workflows and applications for rangeland environments. *Remote Sensing, 3*(11), 2529–2551. https://doi.org/10.3390/rs3112529.

Le Gal, H., Philippe, F., Domon, J. M., Gillet, F., Pelloux, J., & Rayon, C. (2015). Cell wall metabolism in response to abiotic stress. *Plants, 4,* 112–166. https://doi.org/10.3390/plants4010112.

Leakey, A. D. B., Uribelarrea, M., Ainsworth, E. A., Naidu, S. L., Rogers, A., Ort, D. R., et al. (2006). Photosynthesis, productivity, and yield of maize are not affected by open-air elevation of CO_2 concentration in the absence of drought. *Plant Physiology, 140*(2), 779–790. https://doi.org/10.1104/pp.105.073957.

Lizotte, P. L., & Savoie, P. (2013). Spring harvest of corn stover for animal bedding with a self-loading wagon (Article). *Applied Engineering in Agriculture, 29*(1), 25–31.

Long, S. P., Ainsworth, E. A., Leakey, A. D. B., Nosberger, J., & Ort, D. R. (2006). Food for thought: Lower-than-expected crop yield stimulation with rising CO_2 concentrations. *Science, 312*(5782), 1918–1921. https://doi.org/10.1126/science.1114722.

Ma, B. L., Morrison, M. J., & Dwyer, L. M. (1996). Canopy light reflectance and field greenness to assess nitrogen fertilization and yield of maize. *Agronomy Journal, 88*(6), 915–920.

Mansouri-Far, C., Sanavy, S., & Saberali, S. F. (2010). Maize yield response to deficit irrigation during low-sensitive growth stages and nitrogen rate under semi-arid climatic conditions. *Agricultural Water Management, 97*(1), 12–22. https://doi.org/10.1016/j.agwat.2009.08.003.

Mickelbart, M. V., Hasegawa, P. M., & Bailey-Serres, J. (2015). Genetic mechanisms of abiotic stress tolerance that translate to crop yield stability. *Nature Reviews Genetics, 16*(4), 237–251. https://doi.org/10.1038/nrg3901.

Musumarra, G., Barresi, V., Condorelli, D. F., Fortuna, C. G., & Scire, S. (2004). Potentialities of multivariate approaches in genome-based cancer research: identification of candidate genes for new diagnostics by PLS discriminant analysis. *Journal of Chemometrics, 18*(3–4), 125–132. https://doi.org/10.1002/cem.846.

Najafinezhad, H., Sarvestani, Z. T., Sanavy, S., & Naghavi, H. (2015). Evaluation of yield and some physiological changes in corn and sorghum under irrigation regimes and application of barley residue, zeolite and superabsorbent polymer. *Archives of Agronomy and Soil Science, 61*(7), 891–906. https://doi.org/10.1080/03650340.2014.959938.

Nguyen, H. T., & Lee, B. W. (2006). Assessment of rice leaf growth and nitrogen status by hyperspectral canopy reflectance and partial least square regression. *European Journal of Agronomy, 24*(4), 349–356.

Nguy-Robertson, A., Gitelson, A., Peng, Y., Walter-Shea, E., Leavitt, B., & Arkebauer, T. (2013). Continuous monitoring of crop reflectance, vegetation fraction, and identification of developmental stages using a four band radiometer. *Agronomy Journal, 105*(6), 1769–1779. https://doi.org/10.2134/agronj2013.0242.

Norman, J. M., & Jarvis, P. G. (1975). Photosynthesis in Sitka spruce (*Picea sitchensis* (Bong.) Carr.): V. radiation penetration theory and a test case. *Journal of Applied Ecology, 12*(3), 839–878. https://doi.org/10.2307/2402094.

Penuelas, J., Baret, F., & Filella, I. (1995). Semi-empirical indices to assess carotenoids/chlorophyll-a ratio from leaf spectral reflectance. *Photosynthetica, 31*(2), 221–230.

Ray, D. K., Gerber, J. S., MacDonald, G. K., & West, P. C. (2015). Climate variation explains a third of global crop yield variability. *Nature Communications*. https://doi.org/10.1038/ncomms6989.

Rey-Carames, C., Diago, M. P., Martin, M. P., Lobo, A., & Tardaguila, J. (2015). Using RPAS multi-spectral imagery to characterise vigour, leaf development, yield components and berry composition variability within a vineyard. *Remote Sensing, 7*(11), 14458–14481. https://doi.org/10.3390/rs71114458.

Rondeaux, G., Steven, M., & Baret, F. (1996). Optimization of soil-adjusted vegetation indices. *Remote Sensing of Environment, 55*(2), 95–107.

Rouse, J. W., Haas, R. H., Schell, J. A., & Deering, D. W. (1973) Monitoring vegetation systems in the Great Plains with ERTS In *Third Earth Resources Technology Satellite -1*. December. Goddard Space Flight Center: NASA pp. 309–317.

Sanchez, R. A., Hall, A. J., Trapani, N., & Dehunau, R. C. (1983). Effects of water stress on the chlorophyll content, nitrogen level and photosynthesis of leaves of two maize genotypes. *Photosynthesis Research, 4*(1), 35–47. https://doi.org/10.1007/bf00041799.

Sankaran, S., Khot, L. R., Espinoza, C. Z., Jarolmasjed, S., Sathuvalli, V. R., Vandemark, G. J., et al. (2015). Low-altitude, high-resolution aerial imaging systems for row and field crop phenotyping: A review. *European Journal of Agronomy, 70,* 112–123. https://doi.org/10.1016/j.eja.2015.07.004.

Shanahan, J. F., Schepers, J. S., Francis, D. D., Varvel, G. E., Wilhelm, W. W., Tringe, J. M., et al. (2001). Use of remote-sensing imagery to estimate corn grain yield. *Agronomy Journal, 93*(3), 583–589.

Tattini, M., Galardi, C., Pinelli, P., Massai, R., Remorini, D., & Agati, G. (2004). Differential accumulation of flavonoids and hydroxycinnamates in leaves of Ligustrum vulgare under excess light and drought stress. *New Phytologist, 163*(3), 547–561. https://doi.org/10.1111/j.1469-8137.2004.01126.x.

Thomason, W. E., Phillips, S. B., & Raymond, F. D. (2007). Defining useful limits for spectral reflectance measures in corn. *Journal of Plant Nutrition, 30*(7–9), 1263–1277. https://doi.org/10.1080/01904160701555176.

Tollenaar, M., & Lee, E. A. (2006). Dissection of physiological processes underlying grain yield in maize by examining genetic improvement and heterosis. *Maydica, 51*(2), 399–408.

Townsend, P. A., Green, R. O., Campbell, P. K., Cavender-Bares, J., Clark, M. L., Couture, J. J., et al. (2016). Global terrestrial ecosystem functioning and biogeochemical processes. Retrieved April 04, 2017, from https://hyspiri.jpl.nasa.gov/downloads/RFI2_HyspIRI_related_160517/RFI2_final_EcosystemTownsendPhilipA.pdf.

Tucker, C. J. (1979). Red and photographic infrared linear combinations for monitoring vegetation. *Remote Sensing of Environment, 8*(2), 127–150.

Vergara-Diaz, O., Zaman-Allah, M. A., Masuka, B., Hornero, A., Zarco-Tejada, P., Prasanna, B. M., et al. (2016). A novel remote sensing approach for prediction of maize yield under different conditions of nitrogen fertilization. *Frontiers in Plant Science*. https://doi.org/10.3389/fpls.2016.00666.

Vina, A., Gitelson, A. A., Rundquist, D. C., Keydan, G., Leavitt, B., & Schepers, J. (2004). Remote sensing—Monitoring maize (*Zea mays* L.) phenology with remote sensing. *Agronomy Journal, 96*(4), 1139–1147.

Wang, X. P., Guo, N., & Wang, J. (2007). Research on hyperspectral reflectance characteristics for spring wheat in rainfed agriculture areas of loess plateau. *Igarss, 1–12,* 3293–3296.

Weber, V. S., Araus, J. L., Cairns, J. E., Sanchez, C., Melchinger, A. E., & Orsini, E. (2012). Prediction of grain yield using reflectance spectra of canopy and leaves in maize plants grown under different water regimes. *Field Crops Research, 128,* 82–90. https://doi.org/10.1016/j.fcr.2011.12.016.

Wise, B. M., Gallagher, N. B., Bro, R., Shaver, J. M., Winding, W., & Koch, R. S. (2006) 'PLS_Toolbox Version 4.0 ' *for use with MATLAB*. May 18, 2015. Wenatchee, WA, USA: Eigenvector Research, Inc., p. 414. Retrieved from http://212.51.214.51/jsurmacki/pliki/zajecia/LMDiT/cw3/PLS_Manual_4.pdf.

Wold, S., Johansson, E., & Cocchi, M. (1993). PLS- partial least squars projections to latent structures. In H. Kubinyi (Ed.), *3D QSAR in drug design: Theory, methods, and applications* (pp. 523–550). Leiden: ESCOM.

Xie, L., Ying, Y., & Ying, T. (2007). Quantification of chlorophyll content and classification of nontransgenic and transgenic tomato leaves using visible/near-infrared diffuse reflectance spectroscopy. *Journal of Agricultural and Food Chemistry, 55*(12), 4645–4650. https://doi.org/10.1021/jf063664m.

Yin, Z. T., Qin, Q. X., Wu, F. F., Zhang, J. M., Chen, T. T., Sun, Q., et al. (2015). Quantitative trait locus mapping of chlorophyll a fluorescence parameters using a recombinant inbred line population in maize. *Euphytica, 205*(1), 25–35. https://doi.org/10.1007/s10681-015-1380-9.

Zadoks, J. C., Chang, T. T., & Konnzak, C. F. (1974). A decimal code for the growth stages in cereals. *Weed Research, 14*(6), 415–421.

Zaman-Allah, M., Vergara, O., Araus, J. L., Tarekegne, A., Magorokosho, C., Zarco-Tejada, P. J., et al. (2015). Unmanned aerial platform-based multi-spectral imaging for field phenotyping of maize. *Plant Methods*. https://doi.org/10.1186/s13007-015-0078-2.